Effects of sputtering pressure and temperature of ITO electrodes on the performance of p-$BaSi_2$/n-Si heterojunction solar cells

Ryota Sugiyama, Yudai Yamashita, Kaoru Toko, and Takashi Suemasu

Institute of Applied Physics, University of Tsukuba, Tsukuba, Ibaraki 305-8573, Japan

Indium-tin-oxide (ITO) layers were deposited on n-Si(111) (resistivity $\rho > 1000$ Ωcm) by radio frequency (RF) magnetron sputtering, and the effects of sputtering pressure (P) and temperature (T_S) on their electrical properties and transmittance spectra were investigated. The electrical conductivity σ of ITO layers reached a maximal of 1.6×10^4 Scm^{-1} at T_S = 370 °C and P = 1.0 Pa. The transmittance spectra of the ITO layers changed significantly depending on P and T_S. We next employed ITO layers as the front contact for p-$BaSi_2$(20 nm)/n-Si(111) (ρ = 1 – 4 Ωcm) heterojunction solar cells, and investigated the influence of the P and T_S on their performance. The energy conversion efficiency reached a maximum (η = 6.6%) at P = 1.0 Pa and T_S = RT and 90 °C, differently from the T_S suitable for ITO films directly on a Si(111) substrate. Deep level transient spectroscopy revealed the presence of defects in the p-$BaSi_2$ side close to the p-$BaSi_2$/n-Si interface, located at 0.16 eV from the conduction band minimum, when sputtered at 230 °C.

1. Introduction

At present, solar photovoltaic generation has been attracting attention as a clean energy source to replace conventional fossil fuels such as coal and oil. Silicon (Si), which is abundant on earth and has physical properties suitable for solar cells, has long been studied, and now accounts for approximately 90% of the market. The performance of crystal Si (c-Si) solar cells have been improved year by year, and the conversion efficiency (η) is approaching to the theoretical limit determined by its bandgap (E_g).[1] Therefore, the exploration of alternative materials for solar cell applications is of great importance. Among various materials such as cadmium telluride, chalcopyrite, perovskite,[2-6] we have focused on barium disilicide ($BaSi_2$).[7] $BaSi_2$ is composed of earth-abundant elements, and has an E_g of 1.3 eV suitable for a single-junction solar cell, and the absorption coefficient α exceeds 3×10^4 cm^{-1} at a photon energy of 1.5 eV, which is 40 times larger than c-Si.[8-11] The minority-carrier diffusion length, L, of $BaSi_2$ films is about 10 μm,[12] and the minority-carrier lifetime has been improved greatly to over 15 μs by surface passivation with amorphous Si (a-Si) and AlO_x layers[13-16] and by hydrogen passivation.[17] These values are sufficiently large for thin-film solar cell applications. We fabricated p-$BaSi_2$/n-Si heterojunction solar cells consisting of a 20-nm-thick B-doped p-$BaSi_2$ epitaxial layer ($p \sim 2 \times 10^{18}$ cm^{-3}) on n-Si(111) by molecular beam epitaxy (MBE), whereby the η reached 9.9%.[18,19] We also demonstrated the operation of $BaSi_2$ homojunction solar cells very recently.[20] In these $BaSi_2$ solar cells, indium-tin-oxide (ITO) layers deposited by radio-frequency (RF) magnetron sputtering have been used as the front contact layer to collect currents. ITO is a wide band gap (E_g = 3.5 – 4.3 eV) n-type semiconductor having a high light transmittance in the visible wavelength region and a good electrical conductivity. A high electron concentration in ITO films comes from intrinsic point defects such as oxygen vacancies and/or substitution of In^{3+} ions with Sn^{4+} ions.[21] Because of its superior characteristics, ITO films have been widely used in liquid crystal displays, touch panels, solar cells, etc., and are most widely used as a transparent conductive oxide. The ITO film can be formed by various methods such as direct-

current sputtering, RF magnetron sputtering, electron-beam evaporation, chemical vapor deposition and the like. However, it is well known that the deposition conditions greatly affect not only the electrical and transmittance properties of ITO layers, but also the underlayers.[22-24] In Si solar cells, there have been reports showing that the solar cell performance depends on the deposition conditions of ITO layers.[25-28] For example, in heterojunction Si with intrinsic thin layer solar cells,[26] ITO electrodes deposited at room temperature (RT), lead to a very low open-circuit voltage V_{OC} due to the passivation degradation of thin-film hydrogenated a-Si layers underneath probably resulting from particle bombardment during the ITO sputtering. Therefore, ITO sputtering is performed at elevated temperatures like 180 °C to recover some of the degradation induced by the ITO sputtering, resulting in an improvement of V_{OC}. However, there have been no such studies thus far on the performance of $BaSi_2$ solar cells. The purpose of this work is to find the optimum sputtering conditions of ITO layers for $BaSi_2$ solar cells.

In this study, we first investigated the influences of a deposition pressure P and temperature T_S on the properties of ITO films formed on Si substrates by RF magnetron sputtering. Among various sputtering conditions, P and T_S were chosen in this work. This is because it was found that these two parameters significantly increased the electrical conductivity σ of ITO layers compared to other parameters such as power density and oxygen content. We next investigated the effect of P and T_S on the performance of p-$BaSi_2$/n-Si heterojunction solar cells. We also discuss the defects induced around the heterointerface by deep level transient spectroscopy (DLTS).

2. Experiment

Firstly, ITO films were deposited on a float zone (FZ) n-Si(111) substrate (resistivity ρ > 1000 Ωcm) using RF magnetron sputtering. As a target material, ITO pellets made of 90 wt.% In_2O_3 and 10 wt.% SnO_2 were used. After cleaning the Si substrate, ITO films was deposited in a thickness range 80 – 300 nm under a base pressure of 10^{-4} Pa, while the RF power was set at

50 W, and the Ar flow rate was set at 12 sccm. During sputtering, we set T_S at RT and varied P from 0.2 to 3.0 Pa. As described later, the σ of ITO films reached a maximal at P = 1.0 Pa. Thus, we next set P at 1.0 Pa and changed T_S from RT to 370 °C, which is the highest temperature available in the present work. Secondly, we grew p-$BaSi_2$(20 nm) films epitaxially on a Czochralski (CZ) n-Si(111) substrate (resistivity ρ = 1 – 4 Ωcm) by MBE (AVC Co., Ltd) to make p-$BaSi_2$/n-Si heterojunction solar cells.[18,19] After heating the substrates at 900 °C in an ultrahigh vacuum–chamber, a 5-nm-thick $BaSi_2$ template layer serving as a seed crystal was formed by reactive deposition epitaxy (RDE) in which Ba is deposited on a heated Si substrate at 500 °C.[29] Ba deposition rate (R_{Ba}) was 1 nm/min during RDE. After that, T_S was set at 600 °C, and B-doped p-$BaSi_2$ (20 nm, $p \sim 2 \times 10^{18}$ cm^{-3}) was formed by MBE in which Ba, Si, and B were co-evaporated. Finally, a 3-nm-thick a-Si layer was deposited *in situ* on the surface at 180 °C as a passivation film.[30] ITO electrodes with a diameter of 1 nm and thickness of 80 nm were produced on the surface by RF sputtering, and 150 nm Al electrodes were produced on the back surface. For the deposition of ITO electrodes, T_S was fixed at RT and P was changed from 0.2 to 3.0 Pa. As described later, the η reached a maximum at P = 1.0 Pa. Thus, we next changed T_S from RT to 370 °C with keeping P = 1.0 Pa.

The crystalline quality of the ITO layers was characterized by X-ray diffraction (XRD) with a Cu Kα radiation source. The electrical properties were measured by Hall measurement. Solar cell performance was also characterized using a mask with a 1-mm-diameter hole under standard AM1.5 conditions at 25 °C. Photoresponse and transmittance spectra were measured using a lock-in technique with a xenon lamp and a 25 cm focal-length single monochromator (Bunko Keiki, SM-1700A and RU-60N). The light intensity was calibrated with a pyroelectric sensor (Melles Griot, 13PEM001/J). White-bias light was not used. Hall measurement was performed at a magnetic field of 0.73 T, and the Hall voltage was measured at a current of 1 mA. We carried out DLTS measurement in the range 80 – 300 K using a 1 MHz capacitance versus voltage meter (HP 4280A).[31] The rate window was varied between 1 and 512 ms.

3. Results and discussion

3.1 Influence of sputtering conditions on the properties of ITO

a. pressure

Figure 1 shows the P dependences of σ, electron density (n), and electron mobility (μ) of 80-nm-thick ITO films sputtered at RT. With the increase of P, both the n and μ increased, and the σ reached 3.7×10^3 Scm^{-1} at $P = 1.0$ Pa. For higher P, however, the μ started to decreased. As the P increased beyond 2.0 Pa, the n also started to decrease, resulting in $\sigma < 1 \times 10^3$ Scm^{-1} at $P = 3.0$ Pa. The P dependence of grazing-incidence XRD (GI-XRD) patterns of 300-nm-thick ITO films is shown in Fig. 2. At $P \geq 2.0$ Pa, the diffraction peak became apparently broader than those deposited at 0.2 and 1.0 Pa, indicating that the crystalline quality of ITO was degraded. We speculate that's why the μ decreased at $P \geq 2.0$ Pa in Fig. 1.

b. temperature

Figure 3 shows the T_S dependences of σ, n, and μ of 80-nm-thick ITO films. On the basis of the results shown in Fig. 1, we set P at 1.0 Pa and varied T_S in the range RT – 370 °C during sputtering. The σ increased markedly with increasing T_S; it increased up to 1.6×10^4 Scm^{-1} at T_S = 370 °C. Both n and μ increased significantly to 5.3×10^{21} cm^{-3} and 18.8 cm^{2}V^{-1}s^{-1}, respectively, at T_S = 370 °C with increasing T_S. Thereby, this increase of σ is interpreted to originate from the increase of n and μ in ITO films. From the results presented in Figs. 1 and 3, the optimum P and T_S for ITO films on a Si(111) substrate was determined to be 1.0 Pa and 370 °C, respectively.

Figure 4 shows the T_S dependences of transmittance spectra of 80-nm-thick ITO films on a float zone (FZ) n-Si(111) substrate. The P was fixed at 1.0 Pa. As shown in Fig. 4, as T_S was increased, the transmittance maximal near the wavelength of 950 nm at T_S = RT shifted to a shorter wavelength region. This result agrees with the calculation result based on the Drude

model in which the plasma frequency increases as the n increases.[32]

3.2 Influence of sputtering conditions on the performance of p-$BaSi_2$/n-Si heterojunction solar cells

Figure 5 shows the effect of P during ITO sputtering on the current density-voltage (J-V) characteristics of p-$BaSi_2$/n-Si heterojunction solar cells under AM1.5 illumination. T_S was fixed at RT, the same sputtering conditions shown in Fig. 1. The conversion efficiency η increased from 4.7% at P = 0.2 Pa to 5.8% at P = 1.0 Pa, but decreased for further P. Although the short-circuit current density J_{SC} remained almost unchanged, the V_{OC} increased from 0.32 V at P = 0.2 Pa to 0.36 V at P = 1.0 Pa, indicating that the increase of V_{OC} contributed mostly to the enhancement of η. As shown in the internal quantum efficiency (*IQE*) spectra, *IQE* exceeds 80% in the long wavelength range of 800 – 1000 nm regardless of P. Note that *IQE* changed with P in the short wavelength range of 500 – 800 nm. To accurately determine the series resistance (R_S), the shunt resistance (R_{SH}), and the reverse saturation current density (J_0), we adopted a technique described by Sites and Mauk.[33] Using the photodiode equation, the relationship between R_S and R_{SH} can be given as

$$\frac{dV}{dJ} = SR_S + \frac{\gamma k_B T}{q}\left[\frac{1-(SR_{SH})^{-1}\,dV/dJ}{J + J_{SC} - (SR_{SH})^{-1}V}\right], \quad (1),$$

where S is the area of the electrode, γ is the ideality factor, k_B is the Boltzmann constant, T is the absolute temperature, and q is the elemental charge. The solar cell parameters obtained are summarized in Table I.

Table I. Solar cell parameters of the cells with ITO contacts sputtered at RT and at P = 0.2 – 3.0 Pa. Short-circuit current density (J_{SC}), open-circuit voltage (V_{OC}), fill factor (*FF*), conversion efficiency (η), series resistance (R_S), shunt resistance (R_{SH}), and reverse saturation current density (J_0) are all tabulated.

P (Pa)	J_{SC} (mA/cm^2)	V_{OC} (V)	*FF*	η (%)	R_S (Ω)	R_{SH} (kΩ)	J_0 (mA/cm^2)

0.2	26.4	0.33	0.54	4.7	192	82.19	3.71×10^{-3}
1.0	26.7	0.36	0.60	5.8	193	50.75	3.61×10^{-6}
2.0	26.2	0.35	0.58	5.3	244	101.91	2.82×10^{-4}
3.0	26.7	0.35	0.55	5.2	234	116.87	2.13×10^{-5}

For sample with P = 1.0 Pa, the J_0 reached a minimum, and that's why the V_{OC} is the largest among samples. A smaller R_S also contributed to the highest FF among samples; however, the R_S in Table I cannot be explained by the dependence of σ against P in Fig. 1. Therefore, we speculate that the P influences other effects such as collision damage of sputtered species onto the p-$BaSi_2$ films during sputtering and might degrade the quality of the a-Si/p-$BaSi_2$ layers, influencing R_S. Since the η reached a maximal at P = 1.0 Pa in Fig. 5, we next varied the substrate temperature T_S during sputtering.

Figure 6 shows the effects of T_S during sputtering of ITO films on the J-V characteristics of p-$BaSi_2$/n-Si heterojunction solar cells under AM1.5 illumination. The P was fixed at 1.0 Pa and the T_S was varied in the range RT – 370 °C. As shown in Fig. 6, there is not so much difference in the J-V characteristics under AM1.5 illumination between solar cells deposited at T_S = RT and 90 °C when formed at P = 1.0 Pa; η was 6.6% at T_S = RT and 90 °C. On the other hand, the η decreased steadily when the T_S was set at higher than 90 °C. The solar cell parameters are summarized in Fig. 6(b). Note that the data scatter for samples with ITO layers formed at T_S = 230 and 370 °C. When the T_S increased from 90 °C to 230 °C, the V_{OC} was decreased. In contrast, when the T_S was increased further from 230 °C to 370 °C, a recovery of V_{OC} was observed. In addition, J_{SC} decreased and R_S increased greatly, differently from what we anticipated from Fig. 3. We attribute an increase in R_S to the oxidation of p-$BaSi_2$ films by heating upon the deposition of ITO films, and defects generated at the p-$BaSi_2$/n-Si interface.

To investigate the degradation of η in samples with ITO contacts formed at 230 °C (230 °C samples), we performed DLTS measurement on the 230 °C samples. For comparison, samples with ITO contacts formed at RT (RT samples) were also used as a reference. Figure

7(a) is a schematic diagram of DLTS and DLTS profiles. We apply a forward filling pulse voltage (V_P = 0.5 V) to disturb the steady-state reverse-bias condition (V_R = −0.01 V or −1.0 V), which causes the electric field in the depletion region to decrease, and the injection of carriers. We set the pulse width t_{pw} at 50 ms. Due to the difference in carrier concentration between p-$BaSi_2$ and n-Si, the depletion region mostly stretches towards the n-Si side. V_P causes the defect levels to be recharged. When the voltage returns to its steady-state reverse-bias value, trapped carriers emits by thermal emission and thus the defect levels begin to discharge, and the resultant time evolution of the capacitance change $S(T)$ is measured for various rate windows. Whether the detected defects act as minority or majority carrier traps can be immediately determined from the sign of the DLTS signals; positive signals indicate the presence of minority carrier traps, and negative signals indicate the existence of majority carrier traps. In Fig. 7(a), we see an upward facing peak at approximately 120 K for the 230 °C samples. This is due to minority carrier traps. In contrast, there is no such peak for the RT samples. Thus, we can at least state that the 230 °C samples contain more defects than the RT samples, explaining a smaller η. Note that the DLTS peak intensity for the 230 °C samples did not change so much regardless of V_R, indicating that the defect density does not change a lot in the depth direction. The depletion region width is calculated to be approximately 317 nm for n-Si and 0.3 nm for p-$BaSi_2$ at V_R = −0.01 V, and 867 nm and 0.8 nm, respectively, at V_R = −1.0 V. The defect formation in such a deeper region of the n-Si substrate is not likely to occur just by the difference in T_S between RT and 230 °C for ITO contacts. We therefore interpret the upward facing peak in Fig. 7(a) to minority carrier (electron) traps in p-$BaSi_2$ layers. The defect level was calculated to be 0.16 eV from the conduction band minimum, and the defect density is approximately 1.1 × 10^{16} cm^{-3} from the Arrhenius plot in Fig. 7(b). We suppose that a recovery of V_{OC} for the 370 °C samples in Fig. 6(a) might be caused by the decrease of such defects by sputtering at elevated temperatures. On the basis of these results, we conclude that the P during sputtering should be about 1.0 Pa and it is better to deposit at RT – 90 °C when we deposit ITO layers on

p-$BaSi_2$ films. These values of P and T_S cannot be reached only from the formation of ITO layers directly on Si substrates shown in Figs. 1 and 3, suggesting that the presence of collision damage of sputtered species onto the p-$BaSi_2$ films significantly affects the performance of $BaSi_2$ solar cells.

4. Conclusions

We investigated the effects of sputtering pressure P and temperature T_S on the electrical and optical properties of ITO films formed by RF magnetron sputtering. The electrical conductivity σ of ITO layers on Si substrates sputtered at RT increased with P up to 3.7×10^3 Scm^{-1} at P = 1.0 Pa. The σ increased with increasing T_S, and reached a maximum of 1.6×10^4 Scm^{-1} at T_S = 370 °C and P = 1.0 Pa. The transmittance spectra of the ITO layers also depended significantly on P and T_S. We investigated the influence of P and T_S during the sputtering of ITO layers on the performance p-$BaSi_2$(20 nm)/n-Si(111) (ρ = 1 – 4 Ωcm) heterojunction solar cells. It was found that the above mentioned optimum T_S and P were not suitable for p-$BaSi_2$/n-Si solar cells. Differently from expectation, the energy conversion efficiency η reached a maximum (η = 6.6%) at P = 1.0 Pa and T_S = RT and 90 °C. DLTS measurement revealed the generation of electron traps in the p-$BaSi_2$ films, located at 0.16 eV below the conduction band minimum, when the ITO layers were sputtered at T_S = 230 °C and P = 1.0 Pa. These results suggest the $BaSi_2$ films were damaged by collision of sputtered species during the formation of ITO layers by the RF sputtering.

ACKNOWLEDGEMENTS

This work was financially supported by JSPS KAKENHI Grant Numbers 17K18865 and 18H03767 and JST MIRAI. One of the authors (Y.Y.) was financially supported by a Grant-in-Aid for JSPS Fellows (19J21372).

Fig. 1. Sputtering pressure dependences of resistivity, electron density, and mobility of 80-nm-thick ITO films sputtered at RT.

Fig. 2. GI-XRD patterns of 300-nm-thick ITO films sputtered at RT under various values of *P*.

Fig. 3. Sputtering temperature dependences of resistivity, electron density, and mobility of 80-nm-thick ITO films. The pressure during sputtering is 0.2 Pa.

Fig. 4. Sputtering temperature dependences of reflectance spectra of 80-nm-thick ITO films on a float zone (FZ) n-Si(111) substrate. The sputtering pressure is fixed at 1.0 Pa.

Fig. 5. *J–V* characteristics under AM1.5 illumination and *IQE* spectra of p-$BaSi_2$/n-Si heterojunction solar cells with ITO layers sputtered at RT under various pressures.

Fig. 6. (a) *J–V* characteristics and *IQE* spectra of p-$BaSi_2$/n-Si heterojunction solar cells under AM1.5 illumination with ITO layers sputtered at RT–370 °C under P = 1.0 Pa, and (b) their solar cell parameters.

Fig. 7. (a) DLTS profiles obtained for p-$BaSi_2$/n-Si solar cells with ITO layers formed at RT and 230 °C. The forward filling pulse voltage V_p was set at 0.5 V, and the reverse-bias voltage V_R was at –0.01 V or –1.0 V. (b) Arrhenius plot for electron trap level (E1) observed for p-$BaSi_2$/n-Si solar cells with ITO layers formed at 230 °C.

Reference

[1] C.H. Henry, J. Appl. Phys.**51**, 4494 (1980).

[2] P. Jackson, D. Hariskos, R. Wuerz, O. Kiowski, A. Bauer, T. M. Friedlmeier, and M. Powalla, Phys. Stat. Solidi RRL **9,** 28 (2015).

[3] P. Jackson, R. Wuerz, D. Hariskos, E. Lotter, W. Witte, and M. Powalla, Phys. Stat. Solidi RRL **10**, 583 (2016).

[4] X. Wu, Solar Energy **77**, 803 (2004).

[5] J. Burschka, N. Pellet, Soo-Jin Moon, R. Humphry-Baker, P. Gao, M. K. Nazeeruddin, and Michael Grätzel1, Nature **499**, 316 (2013).

[6] W. S. Yang, J. H. Noh, N. J. Jeon, Y. C. Kim, S. Ryu, J. Seo, and S. I. Seok, SCIENCE **348**, 1234 (2015).

[7] T. Suemasu and N. Usami, J. Phys. D **50**, 023001 (2017).

[8] K. Toh, T. Saito, and T. Suemasu, Jpn. J. Appl. Phys. **50**, 068001 (2011).

[9] D. B. Migas, V. L. Shaposhnikov, and V. E. Borisenko, Phys. Status Solidi B **244**, 2611 (2007).

[10] M. Kumar, N. Umezawa, and M. Imai, J. Appl. Phys**. 115**, 203718 (2014).

[11] M. Kumar, N. Umezawa, and M. Imai, Appl. Phys. Express **7**, 071203 (2014).

[12] M. Baba, K. Toh, K. Toko, N. Saito, N. Yoshizawa, K. Jiptner, T. Sakiguchi, K. O. Hara, N. Usami, and T. Suemasu, J. Cryst. Growth **348**, 75 (2012).

[13] K. O. Hara, N. Usami, K. Toh, M. Baba, K. Toko, and T. Suemasu, J. Appl. Phys. **112**, 083108 (2012).

[14] K. O. Hara, N. Usami, K. Nakamura, R. Takabe, M. Baba, K. Toko, and T. Suemasu, Appl. Phys. Express **6**, 112302 (2013).

[15] R. Takabe, K. O. Hara, M. Baba, W. Du, N. Shimada, K. Toko, N. Usami, and T. Suemasu, J. Appl. Phys. **115**, 193510 (2014).

[16] N. M. Shaalan, K. O. Hara, C. T. Trinh, Y. Nakagawa, and N. Usami, Mater. Sci. Semicon. Processing **76**, 37 (2018).

[17] Z. Xu, D. A. Shohonov, A. B. Filonov, K. Gotoh, T. Deng, S. Honda, K. Toko, N. Usami, D. B. Migas, V. E. Borisenko, and T. Suemasu, Phys. Rev. Mater. **3**, 065403 (2019).

[18] S. Yachi, R. Takabe, K. Toko, and T. Suemasu, Appl. Phys. Lett. **109**, 072103 (2016).

[19] T. Deng, T. Sato, Z. Xu, R. Takabe, S. Yachi, Y. Yamashita, K. Toko, and T. Suemasu, Appl. Phys. Express **11**, 062301 (2018).

[20] K. Kodama, Y. Yamashita, K Toko, and T. Suemasu, Appl. Phys. Express **12**, 041005 (2019).

[21] A. Takahashi, Hyomen Gijyutsu **60**, 622 (2009) [Japanese].

[22] S. Ray, R. Banerjee, N. Basu, A. K. Batabyal, and A. K. Barua, J. Appl. Phys**. 54**, 3497 (1983).

[23] Li-jian Meng and M. P. dos Santos, Thin Solid Films **332**, 5662 (1998).

[24] R. Latz, K. Michael, and M. Scherer, Jpn. J. Appl. Phys. **30**, 149151 (1991).

[25] Shui-Yang Lien, Thin Solid Films **518**, S10S13 (2010).

[26] D. Zhang, A. Tavakoliyaraki, Y. Wu, R. A. C. M. M. van Swaaij, and M. Zeman, Energy Procedia **8**, 207213 (2011).

[27] R. Lachaume, W. Favre, P. Scheiblin, X. Garros, N. Nguyen, J. Coignus, D. Munoz, and G. Reimbold, Energy Procedia **38**, 770776 (2013).

[28] M. Tamakoshi, and N. Matsuki, Jpn. J. Appl. Phys. **54**, 08KD09 (2015).

[29] Y. Inomata, Y. Nakamura, T. Suemasu, and F. Hasegawa, Jpn. J. Appl. Phys. **43**, L478 (2004).

[30] R. Takabe, S. Yachi, W. Du, D. Tsukahara, H. Takeuchi, K. Toko, and T. Suemasu, AIP Adv. **6**, 085107 (2016).

[31] D. V. Lang, J. Appl. Phys. **45**, 3023 (1974).

[32] G. Liu, J. B. Kerr, and S. Johnson, Synthetic Metals **144**, 16 (2004).

[33] J. R. Sites and P. H. Mauk, Sol. Cells **27**, 411 (1989).

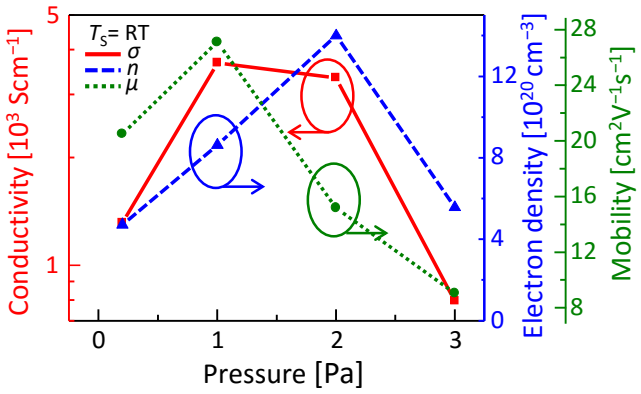
T_S= RT
σ
n
μ
Conductivity [10³ Scm⁻¹]
Electron density [10²⁰ cm⁻³]
Mobility [cm²V⁻¹s⁻¹]
Pressure [Pa]
5
1
0
1
2
3
12
8
4
0
28
24
20
16
12
8

Fig. 1

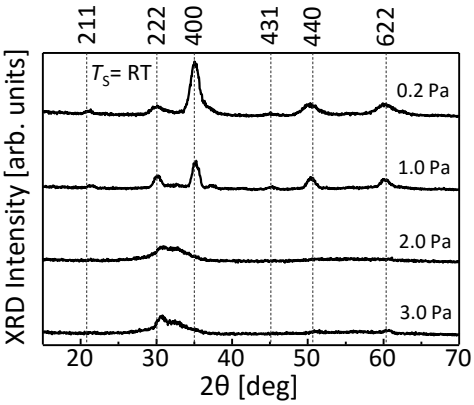
211
222
400
431
440
622
T_S= RT
0.2 Pa
1.0 Pa
2.0 Pa
3.0 Pa
XRD Intensity [arb. units]
20
30
40
50
60
70
2θ [deg]

Fig. 2

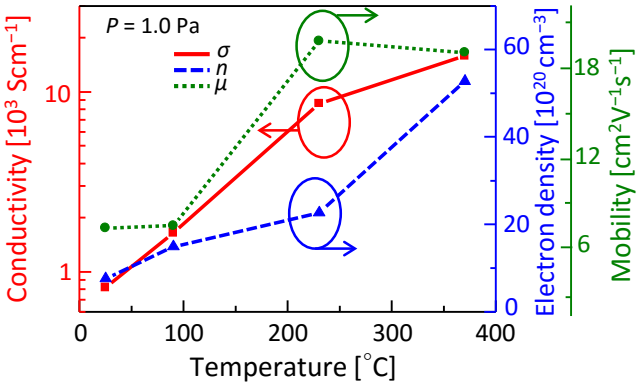
P = 1.0 Pa
σ
n
μ
Conductivity [10³ Scm⁻¹]
Electron density [10²⁰ cm⁻³]
Mobility [cm²V⁻¹s⁻¹]
Temperature [°C]
10
1
60
40
20
0
18
12
6
0
100
200
300
400

Fig. 3

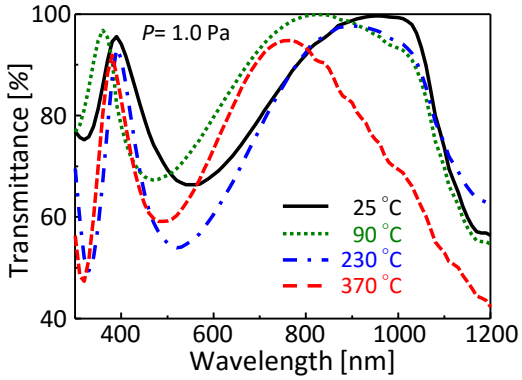
P= 1.0 Pa
Transmittance [%]
Wavelength [nm]
100
80
60
40
400
600
800
1000
1200
25 °C
90 °C
230 °C
370 °C

Fig. 4

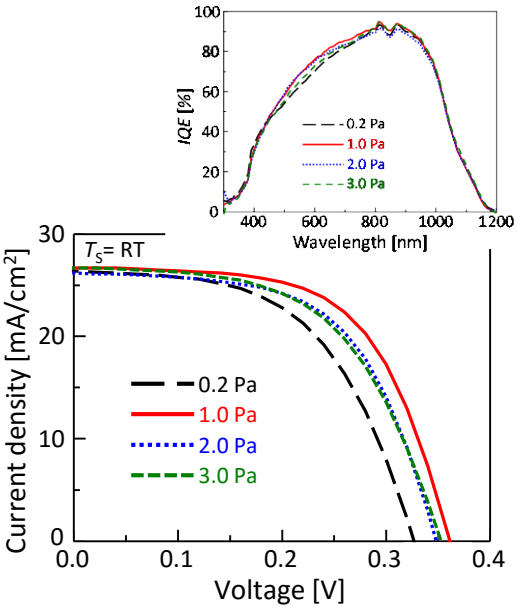
IQE [%]
Wavelength [nm]
0.2 Pa
1.0 Pa
2.0 Pa
3.0 Pa
T_S= RT
Current density [mA/cm^2]
Voltage [V]

Fig. 5

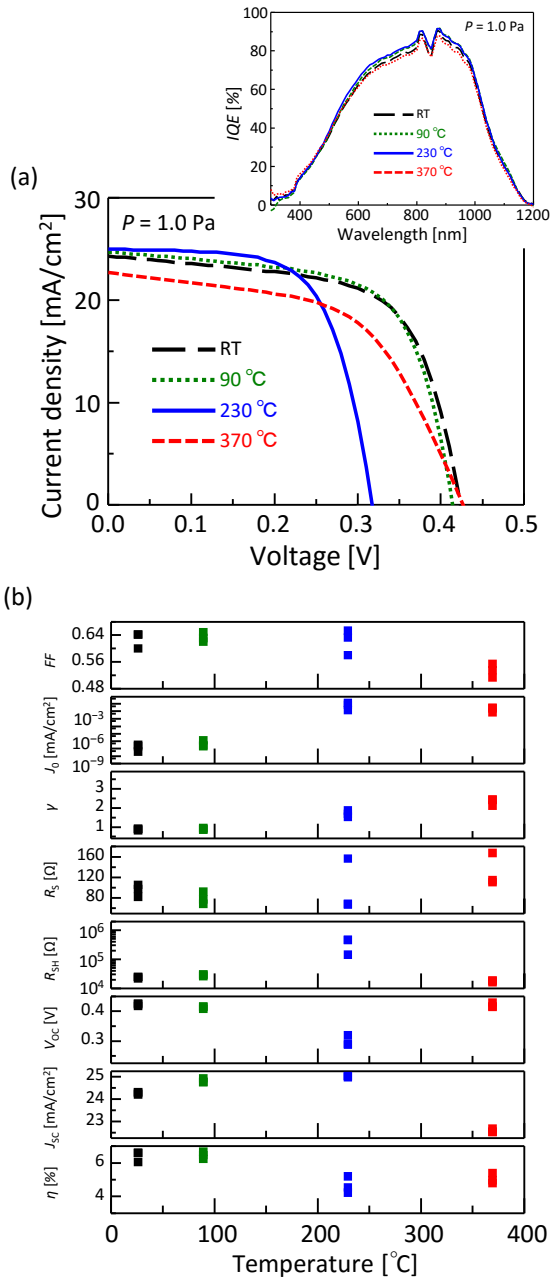
(a)
P = 1.0 Pa
Current density [mA/cm²]
Voltage [V]
RT
90 ℃
230 ℃
370 ℃
IQE [%]
Wavelength [nm]
(b)
FF
J0 [mA/cm²]
γ
RS [Ω]
RSH [Ω]
VOC [V]
JSC [mA/cm²]
η [%]
Temperature [°C]

Fig. 6

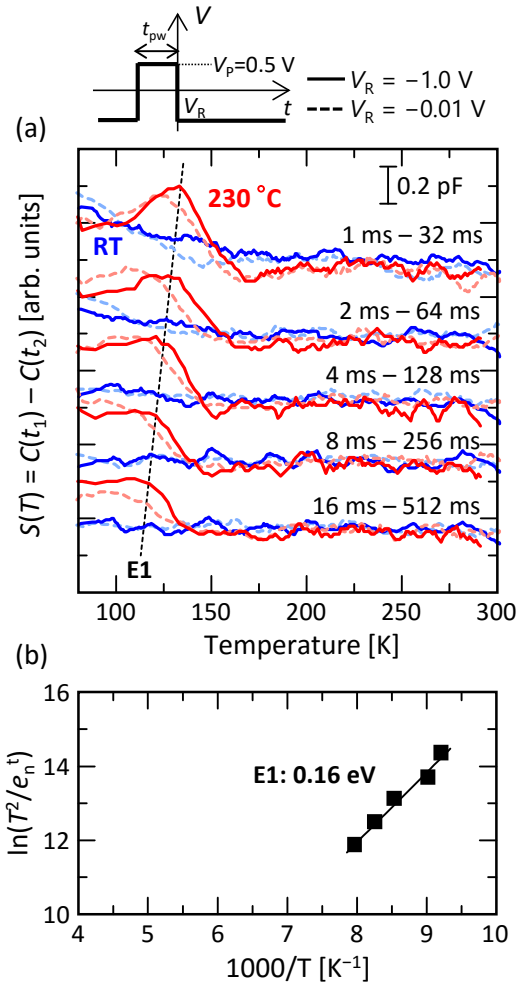
(a)
t_{pw}
V
V_P=0.5 V
V_R
t
V_R = −1.0 V
V_R = −0.01 V
0.2 pF
230 °C
RT
1 ms – 32 ms
2 ms – 64 ms
4 ms – 128 ms
8 ms – 256 ms
16 ms – 512 ms
E1
$S(T) = C(t_1) - C(t_2)$ [arb. units]
100
150
200
250
300
Temperature [K]
(b)
E1: 0.16 eV
$\ln(T^2/e_n^t)$
16
14
12
10
4
5
6
7
8
9
10
1000/T [K^{-1}]

Fig. 7